Sensors and Actuators A 317 (2021) 112442

Contents lists available at ScienceDirect

Sensors and Actuators A: Physical

journal homepage: www.elsevier.com/locate/sna

Curvature, twist and pose measurements using fiber Bragg gratings in multi-core fiber: A comparative study between helical and straight core fibers☆

Fouzia Khan[a,b,*], David Barrera[c], Salvador Sales[d], Sarthak Misra[a,b]

[a] Surgical Robotics Laboratory, Department of Biomedical Engineering, University of Groningen and University of Medical Center Groningen, 9713 GZ, The Netherlands
[b] Department of Biomechanical Engineering, Engineering Technology, University of Twente, 7522 NB, The Netherlands
[c] Department of Electronics, University of Alcalà, Alcalà de Henares 28805, Spain
[d] ITEAM Research Institute, Universitat Politècnica de València, Camino de Vera, 46022 València, Spain

ARTICLE INFO

Article history:
Received 15 July 2020
Received in revised form 4 October 2020
Accepted 13 November 2020
Available online 26 November 2020

Keywords:
Curvature
Twist
Pose
Reconstruction
Fiber Bragg grating
Optical sensing
Elastic rod model
Helical core fiber
Spun core fiber
Twisted core fiber

ABSTRACT

This paper presents a technique to acquire measurements of curvature, twist and pose for two multi-core fibers; one with straight cores and the other with helical cores. Both the fibers have multiple fiber Bragg grating (FBG) sensors inscribed in the cores and the fibers are placed in known configurations in order to compare their measurement accuracy. For the curvature measurements both the fibers are placed in constant curvature slots; for the twist measurements, a set of twists are applied to each fiber and for the pose measurements the fibers are placed in molds of different shape. The mean curvature errors are 0.22 and 0.13 m^{-1}, in the helical and straight core fiber respectively. For the twist measurement the mean errors are 26.57°/m and 146.50°/m in the helical and straight core fiber, respectively. Lastly, the pose measurement consists of position and orientation where the orientation is represented in the axis-angle form. The mean position errors are 0.49 and 0.27 mm, the mean axis orientation errors are 0.12° and 0.26° degrees and the mean angle orientation errors are 1.10° and 1.18°, for the helical and straight core fiber, respectively. The results show that the twist measurement error is significantly low with the helical core fiber, thus helical core fiber is better suited than straight core fiber for applications where twist measurements are required.

1. Introduction

Fiber Bragg gratings (FBG) have been applied in various fields such as oil and gas industry, security, structural health monitoring and have promising applications for monitoring medical instruments [1,2]. This is due to their compactness, light weight, flexibility, tensile strength, immunity to electromagnetic interference and high tolerance to temperature [3]. This study focuses on application of the FBG sensors for curvature, twist and pose measurements of minimally invasive medical instruments. Spatial information of minimally invasive instruments during medical procedures is essential for accurate navigation. The instrument's tip pose, which is the position and orientation, is particularly important for avoiding critical structures inside the body. Currently, this information is commonly acquired using fluoroscopy or ultrasound. However, the instruments can be difficult to observe in ultrasound due to artifacts and low resolution, while fluoroscopy exposes patients to harmful radiation. These issues are mitigated with the use of FBG sensors because they are safe and can provide good resolution data in space and time; thus these sensors are an attractive alternative [4].

In the literature, several studies have validated the use of FBG sensors inscribed in optical fibers for position measurements and its application in medical procedures [1,5–8]. Nevertheless, Duncan et al. have observed error in position measurement from FBG sensors in straight core fiber due to their insufficient sensitivity to twist [9]. In order to acquire more accurate twist measurement

☆ This project has received funding from the European Union's Horizon 2020 research and innovation programme under grant agreement #688279 (EDEN2020). It was also partially supported by the Spanish Ministry of Economy and Competitiveness under the project DIMENSION TEC2017-88029- R. The work of D. Barrera was supported by Spanish MICINN fellowship IJCI-2017-32476. The funding sources were not involved in the research nor in the preparation of the article.

* Corresponding author at: Surgical Robotics Laboratory, Department of Biomedical Engineering, University of Groningen and University of Medical Center Groningen, 9713 GZ, The Netherlands.
E-mail address: f.khan@utwente.nl (F. Khan).

https://doi.org/10.1016/j.sna.2020.112442
0924-4247/

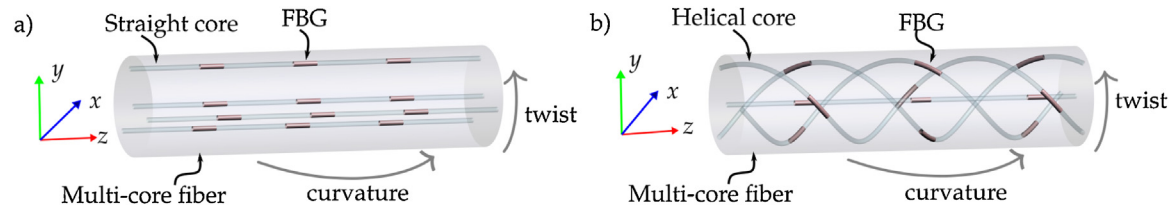

Fig. 1. (a) Straight core fiber with three sets of co-located fiber Bragg grating (FBG) sensors. (b) Helical core fiber with three sets of co-located FBG sensors. Curvature is induced due to a torque about a vector in the x–y plane and twist is due to torque about the z-axis.

researchers have inscribed FBG sensors on helical core fibers and validated its accuracy as twist sensors [3,4,7,10–12]. However, a comparison in measurement accuracy between FBG sensors in helical core fiber and in straight core fiber has not been presented [13]. In this study, the measurement accuracy of curvature, twist and pose are presented for both helical and straight core fiber. Each fiber has multiple sets of co-located FBG sensors as shown in Fig. 1. The results show that the helical core fiber is better suited than the straight core fiber for applications with twist. The main contributions of this study are the application of an elastic rod model to the helical core fiber in order to acquire the pose of the tip and the comparative study of the measurement accuracy between the helical and straight core fiber. The theoretical background utilized to acquire the results, and description of the experiments are presented in Sections 2 and 3, respectively.

2. Theoretical background

The technique to acquire the curvature, twist and pose measurements using FBG sensors in the multi-core fibers with helical and straight cores is presented in this section. It is based on mechanics of materials and the elastic rod theory [14,15]. The curvature and twist is determined from the strain on the fiber. According to the mechanics of materials, the fiber's curvature is related to its normal strain and its twist to its shear strain by the following equations [15]:

$$\epsilon_\kappa = -\kappa y, \tag{1}$$

$$\epsilon_\tau = G\frac{\Delta\phi}{\Delta z}r, \tag{2}$$

where $\epsilon_\kappa \in \mathbb{R}$ is the strain due to curvature, $\kappa \in \mathbb{R}_{\geq 0}$ is the curvature value, $y \in \mathbb{R}_{\geq 0}$ is the perpendicular distance between the neutral axis and the location of the strain on the cross section. The strain due to the twist is $\epsilon_\tau \in \mathbb{R}$ at a radial distance $r \in \mathbb{R}_{>0}$ and $G \in \mathbb{R}_{>0}$ is the material constant relating shear strain with angular difference. The applied twist will cause the cross sections along the arc length of the fiber to rotate with respect to each other. The angular change between two cross sections is given by $\Delta\phi \in \mathbb{R}$ and the difference in arc length between those cross sections is $\Delta z \in \mathbb{R}_{>0}$. $\Delta z = z_2 - z1$ in Fig. 2, which illustrates the variables in (1) and (2) on the multi-core fiber cross-section.

The strains on the fiber can be calculated from the measured Bragg wavelength of the FBG sensors. In this study, the sensors are placed along the fiber such that there are sets of four co-located sensors, which means there are four sensors at particular cross sections of the fiber. These sensors enable measurements of strains at four locations on the cross section, as shown in Fig. 2. These strain measurements can be used to solve for the curvature and twist. The relation between strain and the Bragg wavelength of an FBG sensor can be approximated with the following linear equation [16]:

$$\frac{\Delta\lambda_{B0}}{\lambda_{B0}} = S(\epsilon - \epsilon_0), \tag{3}$$

where $\lambda_{B0} \in \mathbb{R}$ and $\epsilon_0 \in \mathbb{R}$ are the initial values of the Bragg wavelength and strain, respectively. $S \in \mathbb{R}_{>0}$ is the gauge factor and $\epsilon \in \mathbb{R}$ is the strain. However, a general relation that also incorporates the temperature is the following [17]:

$$\ln\frac{\lambda_B}{\lambda_{B0}} = S(\epsilon - \epsilon_0) + \Sigma(T - T_0), \tag{4}$$

where $\lambda_B \in \mathbb{R}$ is the measured Bragg wavelength, $\Sigma \in \mathbb{R}_{>0}$ is the temperature sensitivity, $T \in \mathbb{R}$ is temperature, and $T_0 \in \mathbb{R}$ is the initial temperature.

The strain on the external cores, shown as cores 1–3 in Fig. 2, is due to both curvature and twist; whereas the strain on the central core, labeled 4, is theoretically zero since it is at the center of the cross section. Any change in Bragg wavelength of sensor 4 is due to change in temperature, thus it can be used to eliminate the effect of temperature in cores 1–3. The strain due to twist is the same on the sensors 1–3 and since they are $\frac{2\pi}{3}$ radians apart the mean of the three sensors will give the strain due to twist, see Appendix A for details. The remainder of the strain on cores 1–3 is due to the curvature. Thus, the following equations hold:

$$\epsilon_{i\kappa} = -\kappa r\cos\left(\theta_1 + \frac{2\pi}{3}(i-1)\right), \tag{5}$$

$$\epsilon_\tau = \frac{1}{3S}\sum_{i=1}^{3} m_{i\Delta\epsilon}, \tag{6}$$

where $i \in \{1, b, 3\}$ is the sensor number, $\epsilon_{i\kappa} \in \mathbb{R}$ is the strain due to curvature κ on the FBG sensor in core i, r is the radial distance to the cores, $\theta_1 \in \mathbb{R}$ is the angle between the vector from center to core 1 and the curvature vector $\boldsymbol{v}$, $\epsilon_\tau \in \mathbb{R}$ is the strain on the cores due to twist, S is the gauge factor of the FBG sensors, $m_{i\Delta\epsilon} = m_i - m_4$ and $m_i \in \mathbb{R}$ is $\ln\frac{\lambda_B}{\lambda_{B0}}$, which is the measurement from sensor i. The curvature κ and twist $\Delta\phi$ can be evaluated as:

$$\kappa = \sqrt{v_1^2 + v_2^2}, \tag{7}$$

$$\Delta\phi = \epsilon_\tau\frac{\Delta z}{Gr}, \tag{8}$$

$$\text{where } \boldsymbol{v} = \begin{bmatrix} v_1 \\ v_2 \end{bmatrix} = \begin{bmatrix} \kappa\cos(\theta_1) \\ \kappa\sin(\theta_1) \end{bmatrix} = \mathbf{C}^\dagger\boldsymbol{\zeta}, \quad \mathbf{C} = \begin{bmatrix} -Sr & 0 \\ \frac{1}{2}Sr & \frac{\sqrt{3}}{2}Sr \\ \frac{1}{2}Sr & -\frac{\sqrt{3}}{2}Sr \end{bmatrix}, \quad \boldsymbol{\zeta} = \begin{bmatrix} \zeta_1 \\ \zeta_2 \\ \zeta_3 \end{bmatrix}$$

$\mathbf{C}^\dagger$ is the Moore–Penrose pseudo-inverse of $\mathbf{C}$ and $\zeta_i = m_i - m_4 - S\epsilon_\tau$. Appendix A contains the derivations of (5)–(8).

The fiber's pose can be reconstructed using the curvature vectors and the twist values that are evaluated along its length. Let $n \in \mathbb{Z}_{>0}$ be the number of co-located sets of sensors. Then, the curvature vectors $\boldsymbol{v}[n]$ and twist values $\Delta\phi[n]$ can be acquired using (7) and (8). In this study $\Delta\phi[1]$ is set to be zero. The fiber is modeled as an elastic rod with the center-line represented by a unit-speed curve $\boldsymbol{\gamma}(s) \in \mathbb{R}^3$ and the material frames given by a set of orthonormal vectors $\{\mathbf{d_1}(s) \in \mathbb{R}^3, \mathbf{d_2}(s) \in \mathbb{R}^3, \mathbf{d_3}(s) \in \mathbb{R}^3\}$, where $s \in \mathbb{R}_{\geq 0}$ is the

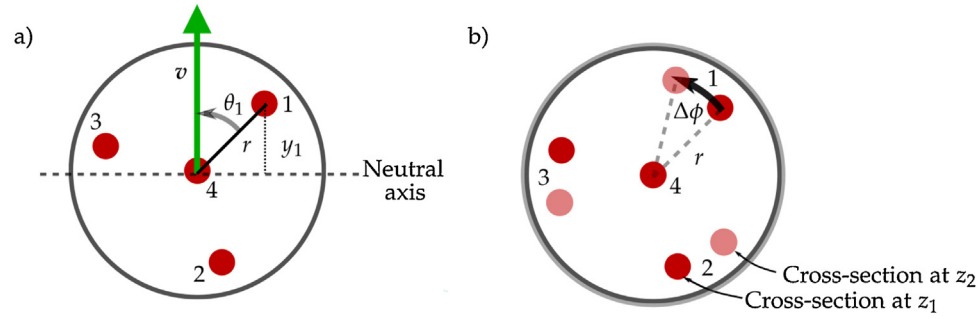

Fig. 2. Cross-section of the straight core fiber and the helical core fiber with numerical labels $\{1, 2, 3, 4\}$ for the cores. (a) Parameters for curvature measurement. $\boldsymbol{v} \in \mathbb{R}^2$ is the curvature vector, $\|\boldsymbol{v}\| = \kappa \in \mathbb{R}$, $\theta_1 \in \mathbb{R}$ is the angle between core 1 and the curvature vector, $r \in \mathbb{R}$ is the radial distance to the cores, $y_1 \in \mathbb{R}$ is the perpendicular distance from core 1 to the neutral axis. (b) Parameters for twist measurement. Overlay of two cross sections of the fiber, one at arc length $z_1 \in \mathbb{R}_{>0}$ and the other at $z_2 \in \mathbb{R}_{>0}$, $\Delta z = z_2 - z_1$. An applied twist will cause the cross sections to be rotated with respect to each other, this rotation is $\Delta\phi \in \mathbb{R}$.

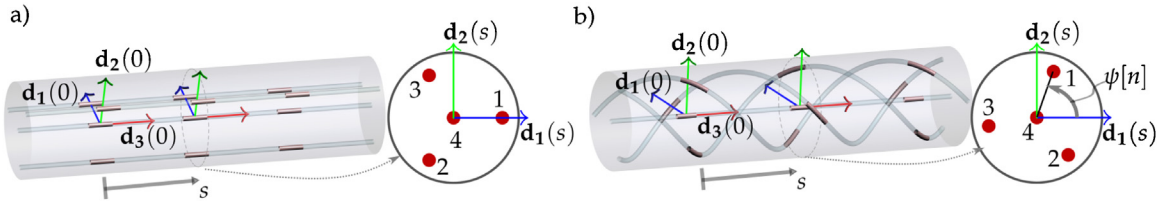

Fig. 3. Schematic of the straight core fiber and the helical core fiber with the material frames $\{\mathrm{d_1}(s) \in \mathbb{R}^3, \mathrm{d_2}(s) \in \mathbb{R}^3, \mathrm{d_3}(s) \in \mathbb{R}^3\}$ are shown in a) and b), respectively. The arc length of the fiber is parameterized by $s \in \mathbb{R}$, the sensor set number is parameterized by $n \in \mathbb{Z}$, $\psi[n] \in \mathbb{R}$ is the angle between $\mathrm{d_1}$ and core 1 in set n.

parameter for the arc length of the fiber, as illustrated in Fig. 3. The equations for an elastic rod are as follows:

$$\frac{\mathrm{d}}{\mathrm{d}s}\boldsymbol{\gamma}(s) = \mathrm{d_3}(s), \tag{9}$$

$$\frac{\mathrm{d}}{\mathrm{d}s}\mathrm{d_1}(s) = \tilde{\phi}(s)\mathrm{d_2}(s) - \tilde{\chi}_2(s)\mathrm{d_3}(s), \tag{10}$$

$$\frac{\mathrm{d}}{\mathrm{d}s}\mathrm{d_2}(s) = -\tilde{\phi}(s)\mathrm{d_1}(s) + \tilde{\chi}_1(s)\mathrm{d_3}(s), \tag{11}$$

$$\frac{\mathrm{d}}{\mathrm{d}s}\mathrm{d_3}(s) = \tilde{\chi}_2(s)\mathrm{d_1}(s) - \tilde{\chi}_1(s)\mathrm{d_2}(s), \tag{12}$$

where $\tilde{\phi}(s) \in \mathbb{R}$, $\tilde{\chi}_1(s) \in \mathbb{R}$ and $\tilde{\chi}_2(s) \in \mathbb{R}$ are the rotations of the center-line $\boldsymbol{\gamma}(s) \in \mathbb{R}^3$ about $\mathrm{d_3}(s)$, $\mathrm{d_1}(s)$ and $\mathrm{d_2}(s)$, respectively [14]. These rotations are related to the curvature $\boldsymbol{v}[n]$ and twist $\Delta\phi[n]$ calculated from the FBG sensors. For both the helical and straight core fiber, linearly interpolating $\Delta\phi[n]$ over the arc length s gives the rotation about $\mathrm{d_3}(s)$ which is $\tilde{\phi}(s)$. Similarly, for the straight core fiber, linear interpolation of $v_1[n]$ and $v_2[n]$ gives $\tilde{\chi}_1(s)$ and $\tilde{\chi}_2(s)$, respectively. However, for the helical core fiber since $\mathrm{d_1}(s)$ does not coincide with core 1 for all s, the calculated curvature vector $\boldsymbol{v}[n]$ must be adjusted such that it is with respect to the material frame. This is achieved by subtracting the angle $\psi[n] \in \mathbb{R}$ between $\mathrm{d_1}$ and core 1 on cross-section of the sensor set n from $\theta_1[n]$, see Fig. 3. The angle $\psi[n]$ is related to the rate at which the fiber is twisted in order to create the helical cores. Thus, $\psi[n]$ can be either calculated from the twist rate or deduced experimentally. For the helical core fiber $\tilde{\chi}_1(s)$ and $\tilde{\chi}_2(s)$ are interpolation of $\chi_1[n] = \kappa[n]\cos(\theta_1[n] - \psi[n])$ and $\chi_2[n] = \kappa[n]\sin(\theta_1[n] - \psi[n])$, respectively. Then, the pose of both the fibers can be acquired using the discretized solution of (9)–(12) which is:

$$\mathbf{X}(s + \Delta s) = \mathbf{X}(s)\exp\left(\mathbf{A}(s)\Delta s\right), \tag{13}$$

where $\mathbf{X}(s) = \begin{bmatrix} \mathrm{d_1}(s) & \mathrm{d_2}(s) & \mathrm{d_3}(s) & \boldsymbol{\gamma}(s) \\ 0 & 0 & 0 & 1 \end{bmatrix}$,

$$\mathbf{A}(s) = \begin{bmatrix} 0 & -\tilde{\phi}(s) & \tilde{\chi}_2(s) & 0 \\ \tilde{\phi}(s) & 0 & -\tilde{\chi}_1(s) & 0 \\ -\tilde{\chi}_2(s) & \tilde{\chi}_1(s) & 0 & 1 \\ 0 & 0 & 0 & 0 \end{bmatrix},$$

$\boldsymbol{\gamma}(0) = [0\ \ 0\ \ 0]^{\mathrm{T}}$, $\mathrm{d_1}(0) = [1\ \ 0\ \ 0]^{\mathrm{T}}$, $\mathrm{d_2}(0) = [0\ \ 1\ \ 0]^{\mathrm{T}}$, and $\mathrm{d_3}(0) = [0\ \ 0\ \ 1]^{\mathrm{T}}$ [18]. The fiber tip position is $\boldsymbol{\gamma}(L)$ and tip orientation in matrix form is $[\mathrm{d_1}(L)\ \ \mathrm{d_2}(L)\ \ \mathrm{d_3}(L)]$, where L is the length of the fiber. The equations for acquiring the curvature, twist and pose measurements are validated through a set of experiments which are presented in the next section.

3. Experiments and results

The equations presented in the previous section are utilized in three experiments that are conducted to compare the curvature, twist, and pose measurement accuracy between two multi-core fibers, one with helical cores and another with straight cores. The FBG sensors in both the fibers are inscribed using phase masks and ultra-violet laser. They are inscribed in the multi-core fiber with straight cores in-house and in the multi-core fiber with helical cores by Fujikura (Tokyo, Japan). Table 1 lists the specifications of the fibers. The insertion loss of the straight core fiber including the fan-out is 1.5 dB and of the helical core fiber including the fan out is 2.2 dB. There are 8 sets of FBG sensors, where each set consists of four co-located sensors that have the same Bragg wavelength. In the straight core fiber, the Bragg wavelengths range from 1537 to 1554 nm with an increment of approximately 2 nm. In the helical core fiber, the Bragg wavelengths range from 1542 to 1556 nm with an increment of approximately 2 nm. The light source and the spectrum analyzer for the sensors are provided by the interrogator

Table 1
Specifications of the straight and helical multi-core fibers.

Core	Sensorized length	FBG length	Twist rate	Center to core
Helical	175 mm	11 mm	50 turns/m	35 μm
Straight	115.5 mm	10 mm	N/A	35 μm

Core	Cladding diameter	Coating diameter	Core angles	Coating type
Helical	125 μm	200 μm	120°	Acrylate
Straight	125 μm	250 μm	120°	Acrylate

FBG-804D (FBGS International NV, Geel). The wavelength data is processed offline in Matlab 2017b (MathWorks, Massachusetts).

3.1. Curvature

The experiments for curvature accuracy utilizes an acrylic board with seven fixed curvature slots that range from 1.33 to 5.71 m^{-1}. These slots are created using laser cutter and then smoothened by fine sandpaper. Fig. 4a shows a photograph of the board. The accuracy of the two fibers are evaluated by placing them in the slots and getting the difference between the measured curvature and the curvature of the slot. Fig. 5a plots each slot's curvature as the ground truth and the corresponding calculated curvature using (7), where r is the center to core distance of the fiber and S is determined through calibration for each FBG set. The calibration procedure consists of collecting measurements from the fiber and solving for the value of S that leads to the minimum difference between the measurements and the ground truth. The curvature error measure $\kappa_e \in \mathbb{R}_{\geq 0}$ utilized is the absolute difference between the ground truth $\kappa_{gt} \in \mathbb{R}_{\geq 0}$ and the measured curvature $\kappa_m \in \mathbb{R}_{\geq 0}$:

$$\kappa_e = |\kappa_{gt} - \kappa_m|, \tag{14}$$

The error κ_e is calculated for each sensor set and the mean error of the sensor sets over all the slots is 0.22 and 0.13 m^{-1} for helical and straight core fiber, respectively. The standard deviation of the error is 0.11 and 0.07 m^{-1} for helical and straight core fiber, respectively. The results show that the straight core fiber is more accurate in measuring the curvature however not significantly more. One source of inaccuracy in the helical fiber could be due to multiple peaks reflected from the sensors when the slot curvature is greater than 4 m^{-1}. For this study the mean of the multi-peaks is considered to be the shifted Bragg wavelength. Fig. 5b illustrates a spectra, where one of the sensors has double peaks. The phenomenon of multiple peaks may be reduced by using apodized FBG sensors.

3.2. Twist

The accuracy of measuring twist using the two fibers is determined by clamping one end of the fiber and applying a rotation at the other end, which is the tip of the fiber. This experiment is conducted using an in-house assembled cage mechanism, as shown in Fig. 4b. The rotating end of the mechanism consists of a dial with angular graduations of five degrees. During the experiment, the fiber is clamped on both ends and the dial is rotated in steps of 10° from 10° to 90° in clockwise (CW) and counter-clockwise (CCW) directions, as shown in Fig. 4b. The error in twist measurement $\phi_e \in \mathbb{R}$ is determined by the absolute difference between the applied twist $\phi_{app} \in \mathbb{R}$ and the measured twist $\phi_m \in \mathbb{R}$ as per the following equation:

$$\phi_e = |\phi_{app} - \phi_m|, \tag{15}$$

The measured twist ϕ_m is calculated using (8), where Δz is the distance between the FBG sensor sets, r is the center to core distance. G is determined by calibration where a set of experiment data is used to find the value of G for which the twist error is minimized. Fig. 6 shows the plot of the ground truth, which is the applied twist, and the measured twist for both the straight and helical core fiber. The applied twist along the fiber is related to the tip rotation as: $\phi_{app} = \theta_t / L$ where, $\theta_t \in \mathbb{R}$ is the tip rotation and L is 175 mm since that is the fiber length over which the twist is applied. The mean twist error is 26.57°/m and 146.50°/m for helical and straight core fibers, respectively. The standard deviation in twist error is 29.96°/m and 59.74°/m for helical and straight core fibers, respectively.

The results show that the helical core fiber can measure the twist with more accuracy than the straight core fiber. This is because with the straight core the FBG sensing of shear strain is very low whereas in helical core since the FBGs are on a helix the twist translates into elongation thus the FBG sensors register the shear strain more accurately. Another observation is that the helical core fiber does not have a symmetric response for clockwise and counter-clockwise twist. This could be due to the non-symmetric response of the sensors to elongation and compression.

Table 2
The mean and standard deviation in brackets over multiple trials of the position, axis and angle error according to (16)– (18), respectively.

	Helical	Straight
r_e (mm)	0.49 (0.24)	0.27 (0.14)
v_e (°)	0.12 (0.16)	0.26 (0.14)
ω_e (°)	1.10 (0.71)	1.18 (1.06)

3.3. Pose

In this experiment, each of the two fibers is placed in a catheter which is then placed in three molds with the following center-line curve: arc, S curve and 3D curve, as shown in Fig. 4c. The arc is a planar curve with a constant curvature of 3.33 m^{-1}, the S curve is also a planar curve with curvature changing from 2.5 to −2.5 m^{-1}, lastly the 3D curve is a segment of a helix with radius of 0.1 m and pitch of 2.05×10^{-1} m. Thus, the tip pose of the three curves are known and utilized as ground truths. The tip pose of the fiber is acquired using (13), where $\psi[n]$ is found by placing the fiber in a fixed curvature slot and calculating the difference between the measured frame and the actual frame. Moreover, the fiber tip position $\mathbf{r} \in \mathbb{R}^3$ is $\boldsymbol{\gamma}(L)$, where L is the length from the first sensor set to the last. The orientation of the fiber tip is given by the material frames $\mathbf{d_1}$, $\mathbf{d_2}$, $\mathbf{d_3}$, since they are orthonormal they form an orientation matrix and the orientation at the tip is given by the matrix $[\mathbf{d_1}(L)\ \ \mathbf{d_2}(L)\ \ \mathbf{d_3}(L)]$. For error calculations we use axis-angle representation of orientation that is derived from the tip orientation matrix [19]. The axis which is the tip orientation vector is given as $\mathbf{v} \in \mathbb{R}^3$ and the angle which is the angle of rotation about the orientation vector is given as $\omega \in \mathbb{R}$. The pose error measures are calculated as follows [18]:

$$r_e = \|\mathbf{r} - \mathbf{r}_{gt}\|, \tag{16}$$

$$\mathrm{v}_e = \cos^{-1}\left(\frac{\mathbf{v}_{gt} \cdot \mathbf{v}}{\|\mathbf{v}_{gt}\|\|\mathbf{v}\|}\right), \tag{17}$$

$$\omega_e = \|\omega - \omega_{gt}\|, \tag{18}$$

where $\mathbf{r}_{gt} \in \mathbb{R}^3$ is the ground truth of the tip position, $\mathbf{v}_{gt} \in \mathbb{R}^3$ is the true orientation vector and $\omega_{gt} \in \mathbb{R}$ is the angle of rotation about the true orientation vector. The catheter with the fiber is inserted in each mold five times. Table 2 gives the mean pose errors and the standard deviation over all the trials. Fig. 7 shows the reconstructions of the three curves and the tip pose for one of the trials. The results show that both the fibers have similar error measures, however the helical core fiber gives a slightly lower error in orientation for the space curve pose.

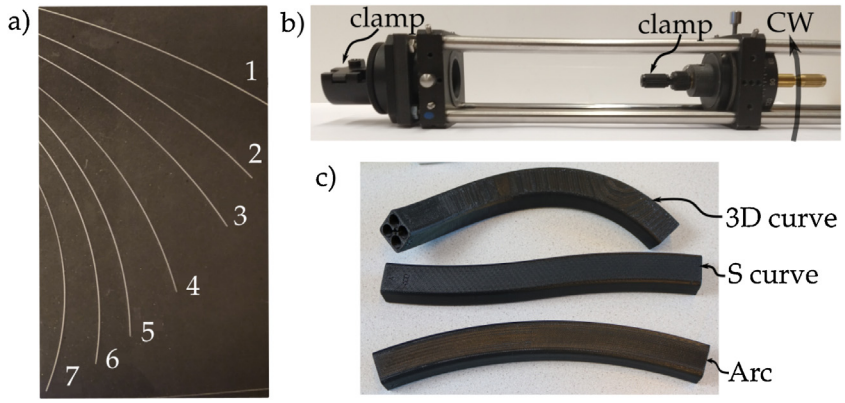

Fig. 4. (a) Slots of fixed curvature on an acrylic board used for determining curvature accuracy of the two multi-core fibers. Each slot is numbered and has a unique curvature in the range from 1.33 to 5.71 m^{-1}. (b) A cage mechanism where a fiber can be clamped such that one end is fixed and the other end can be rotated. This setup is utilized for the twist experiments, where the fiber is rotated in clockwise (CW) and counter-clockwise (CCW) directions in steps of 10°. The distance between the two clamps is 175 mm. (c) The three molds used for the pose experiments. The arc has a constant curvature of 3.33 m^{-1}, the S curve has a linearly changing curvature starting from 2.5 to −2.5 m^{-1} and the 3D curve is a helix with radius of 0.1 m and pitch of 2.05×10^{-1} m.

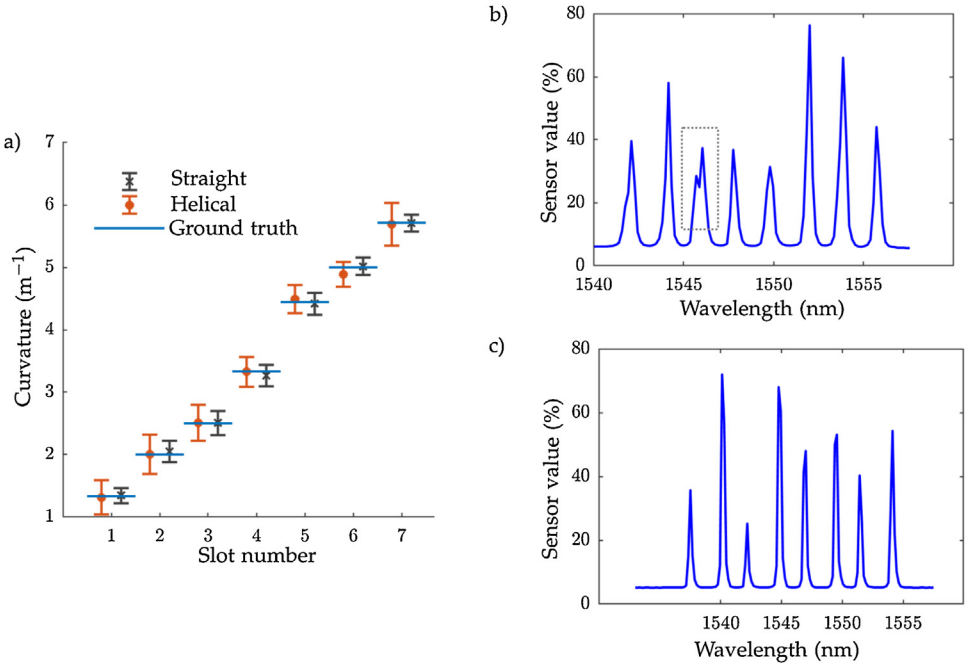

Fig. 5. (a) The mean and standard deviation of the curvature measurements along with the ground truth. The slot number is a unique number given to each slot with fixed curvature and the slot's curvature is the ground truth value. (b) A spectra from fiber Bragg grating sensors on the helical core fiber with double peaks, which are highlighted with a gray dashed box. (c) A spectra from fiber Bragg grating sensors on the straight core fiber.

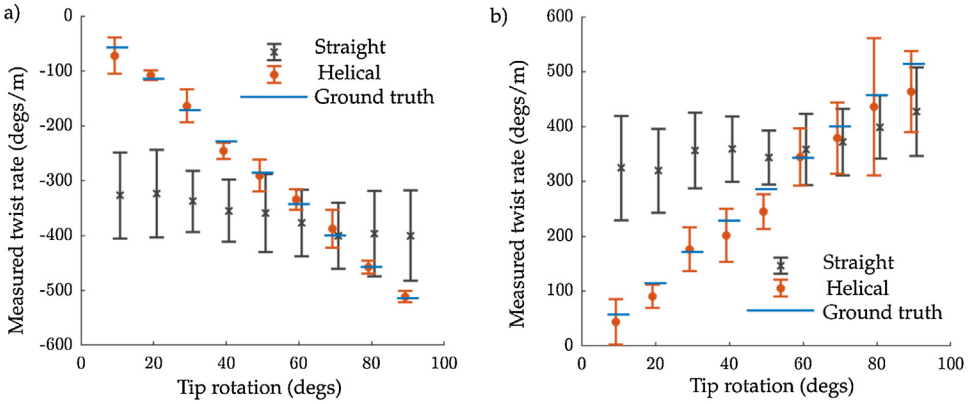

Fig. 6. The mean and standard deviation of the twist measurements in clockwise (a) and counter-clockwise direction (b).

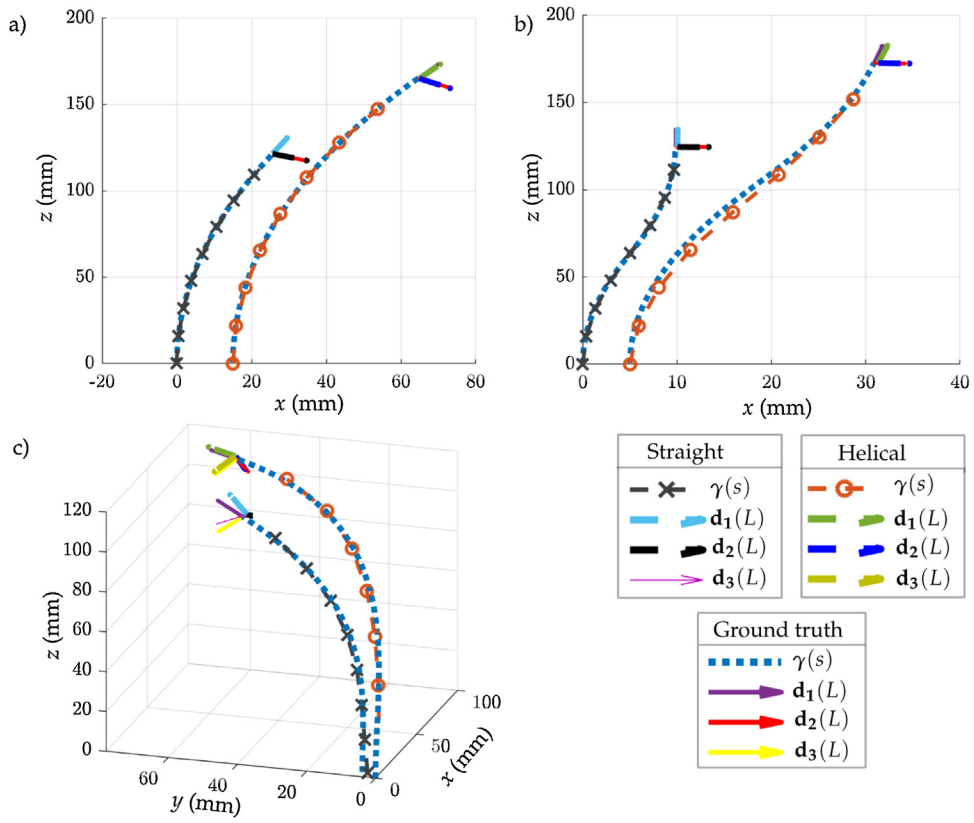

Fig. 7. The pose measurement based on the fiber Bragg grating sensors and the ground truth for the three molds. The helical core measurements in the plots are shifted about the x axis for visual clarity. The curves for the straight core fiber is shorter than the helical core fiber because the sensorized length of the straight and helical core fiber are 115.5 and 175 mm, respectively. The tip pose and the center-line of the straight and helical core fiber for the arc, S curve and 3D curve are shown in (a), (b) and (c), respectively.

4. Conclusions

In this study, multi-core fibers with FBG sensors are utilized to acquire curvature, twist and pose measurements. Moreover, the accuracy of the measurements from the FBG sensors in a helical core fiber is compared to that of the sensors in a straight core fiber. The mean error in curvature for helical and straight core fiber are 0.22 and 0.13 m^{-1}, respectively, whereas in twist measurement the mean error measures are 26.57°/m and 146.50°/m, respectively. Lastly, the mean error in position for the helical and straight core fiber are 0.49 and 0.27 mm, respectively; in axis orientation is 0.12° and 0.26°; and in angle orientation is 1.10° and 1.18°, respectively. The accuracy for the pose measurement is similar for both fibers. However, for applications with twist, FBG sensors on helical core fiber will produce more accurate results than FBG sensors on straight core fiber.

Authors' contribution

Fouzia Khan: conceptualization, methodology, software, validation, formal analysis, investigation, resources, data curation, writing – original draft preparation, writing – review and editing. David Barrera: formal analysis, investigation, resources, writing – review and editing. Salvador Sales: Writing – review and editing, supervision, project administration, funding acquisition. Sarthak Misra: conceptualization, writing – review and editing, supervision, project administration, funding acquisition.

Conflict of interest

None declared.

Declaration of Competing Interest

The authors report no declarations of interest.

Acknowledgements

The authors would like to thank Francis Kalloor Joseph and Frans Segerink from University of Twente for their assistance in building the twist experiment setup. In addition, the authors really appreciate the assistance provided by Fujikura in understanding the spectra from the helical core fibers and by FBGS International NV with the strain to wavelength equation.

Appendix A

The derivation of (5)–(8) is given in this appendix. The curvature and twist are evaluated from the Bragg wavelength measurements of the FBG sensors. First, the strain on the fiber is calculated from the wavelength measurements and then the curvature and twist is evaluated from the strain using material mechanics [15]. The relation between the strain and the wavelength is given in (4) as:

$$\ln \frac{\lambda_B}{\lambda_{B0}} = S(\epsilon - \epsilon_0) + \Sigma(T - T_0), \tag{A.1}$$

The left hand side of (A.1) is a direct measurement from the sensors. Let $i \in \{1, 2, c, 4\}$ represent the FBG sensor number,

$$\ln \frac{\lambda_{Bi}}{\lambda_{B0i}} = m_i, \quad \text{and} \tag{A.2}$$

$$S(\epsilon_i - \epsilon_{0i}) = S(\epsilon_{ik} + \epsilon_\tau) = m_{i\Delta\epsilon}, \tag{A.3}$$

where $m_i \in \mathbb{R}$, (A.3) is based on $\epsilon_{0i} = 0$ which is true if λ_{B0i} is measured when fiber is stress-free. $\epsilon_{i\kappa} \in \mathbb{R}$ is strain due to curvature and ϵ_τ is axial twist strain which is the same in sensors 1, 2 and 3. All four FBG sensors will experience the same temperature change because they are close in proximity, thus the value of the term $\Sigma(T - T_0)$ is the same in all sensors. Moreover, sensor 4 theoretically will be strain free because it is in the center of the fiber, thus:

$$\Sigma(T_i - T_{0i}) = m_4, \tag{A.4}$$

$$\epsilon_{i\kappa} = -\kappa r \cos\left(\theta_1 + \frac{2\pi}{3}(i-1)\right), \tag{A.5}$$

where $\epsilon_{i\kappa} \in \mathbb{R}$ is the strain is sensor $i \in \{1, 2, 3\}$; $\epsilon_{4\kappa} = 0$. (A.5) is based on material mechanics, for further details see Khan et al. [1]. The following holds for sensors $i \in \{1, 2, 3\}$ using (A.2) and (A.3):

$$m_i = m_{i\Delta\epsilon} + m_4 \tag{A.6}$$

Substituting (A.3), (A.5) into (A.6) and applying trigonometric angle sum identities the following holds:

$$m_1 - m_4 = m_{1\Delta\epsilon} = S(-\kappa r \cos(\theta_1) + \epsilon_\tau), \tag{A.7}$$

$$m_2 - m_4 = m_{2\Delta\epsilon} = S\left(\frac{1}{2}\kappa r \cos(\theta_1) + \frac{\sqrt{3}}{2}\sin(\theta_1) + \epsilon_\tau\right), \tag{A.8}$$

$$m_3 - m_4 = m_{3\Delta\epsilon} = S\left(\frac{1}{2}\kappa r \cos(\theta_1) - \frac{\sqrt{3}}{2}\sin(\theta_1) + \epsilon_\tau\right). \tag{A.9}$$

Summing (A.7)–(A.9) leads to the trigonometry terms to add to zero and the following is achieved:

$$\frac{1}{3S}\sum_{i=1}^{3} m_{i\Delta\epsilon} = \epsilon_\tau. \tag{A.10}$$

Thus, the strain due to twist can be calculated using (A.10) and the twist can be calculated by rearranging (2) into:

$$\Delta\phi = \epsilon_\tau \frac{\Delta z}{Gr}, \tag{A.11}$$

which is the twist equation (8). The curvature value can be solved by rearranging (A.7)–(A.9) as

$$\zeta = \mathbf{C}\boldsymbol{v}, \tag{A.12}$$

$$\text{where} \quad \boldsymbol{\zeta} = \begin{bmatrix} \zeta_1 \\ \zeta_2 \\ \zeta_3 \end{bmatrix} = \begin{bmatrix} m_1 - m_4 - S\epsilon_\tau \\ m_2 - m_4 - S\epsilon_\tau \\ m_3 - m_4 - S\epsilon_\tau \end{bmatrix}, \quad \mathbf{C} = \begin{bmatrix} -Sr & 0 \\ \frac{1}{2}Sr & \frac{\sqrt{3}}{2}Sr \\ \frac{1}{2}Sr & -\frac{\sqrt{3}}{2}Sr \end{bmatrix}$$

$$\boldsymbol{v} = \begin{bmatrix} v_1 \\ v_2 \end{bmatrix} = \begin{bmatrix} \kappa\cos(\theta_1) \\ \kappa\sin(\theta_1) \end{bmatrix}$$

Then $v = \mathbf{C}^\dagger\boldsymbol{\zeta}$, where $\mathbf{C}^\dagger$ is the Moore–Penrose pseudo-inverse of $\mathbf{C}$ and

$$\kappa = \|\boldsymbol{v}\| = \sqrt{v_1^2 + v_2^2} \tag{A.13}$$

gives the curvature equation (7).

References

[1] F. Khan, A. Denasi, D. Barrera, J. Madrigal, S. Sales, S. Misra, Multi-core optical fibers with Bragg gratings as shape sensor for flexible medical instruments, IEEE Sens. J. 19 (14) (2019) 5878–5884.

[2] P.S. Westbrook, T. Kremp, K.S. Feder, W. Ko, E.M. Monberg, H. Wu, D.A. Simoff, T.F. Taunay, R.M. Ortiz, Continuous multicore optical fiber grating arrays for distributed sensing applications, J. Lightwave Technol. 35 (6) (2017) 1248–1252.

[3] A. Wolf, A. Dostovalov, K. Bronnikov, S. Babin, Arrays of fiber Bragg gratings selectively inscribed in different cores of 7-core spun optical fiber by IR femtosecond laser pulses, Opt. Express 27 (10) (2019) 13978–13990.

[4] C.G. Askins, G.A. Miller, E.J. Friebele, Bend and twist sensing in a multi-core optical fiber, LEOS 2008-21st Annual Meeting of the IEEE Lasers and Electro-Optics Society (2008) 109–110.

[5] J.P. Moore, M.D. Rogge, Shape sensing using multi-core fiber optic cable and parametric curve solutions, Opt. Express 20 (3) (2012) 2967–2973.

[6] S. Jäckle, T. Eixmann, H. Schulz-Hildebrandt, G. Hüttmann, T. Pätz, Fiber optical shape sensing of flexible instruments for endovascular navigation, Int. J. Comput. Assist. Radiol. Surg. 14 (2019) 2137–2145.

[7] R. Xu, A. Yurkewich, R.V. Patel, Curvature, torsion, and force sensing in continuum robots using helically wrapped FBG sensors, IEEE Robot. Autom. Lett. 1 (2) (2016) 1052–1059.

[8] R.J. Roesthuis, M. Kemp, J.J. van den Dobbelsteen, S. Misra, Three-dimensional needle shape reconstruction using an array of fiber Bragg grating sensors, IEEE/ASME Trans. Mechatron. 19 (4) (2014) 1115–1126.

[9] R.G. Duncan, M.T. Raum, Characterization of a fiber-optic shape and position sensor, Smart Structures and Materials 2006: Smart Sensor Monitoring Systems and Applications (2006) 26–36.

[10] Y. Wang, C. Xu, V. Izraelian, Bragg gratings in spun fibers, IEEE Photon. Technol. Lett. 17 (6) (2005) 1220–1222.

[11] H. Zhang, Z. Wu, P.P. Shum, X. Shao, R. Wang, X.Q. Dinh, S. Fu, W. Tong, M. Tang, Directional torsion and temperature discrimination based on a multicore fiber with a helical structure, Opt. Express 26 (1) (2018) 544–551.

[12] I. Floris, J. Madrigal, S. Sales, P.A. Calderòn, J.M. Adam, Twisting compensation of optical multicore fiber shape sensors for flexible medical instruments, Optical Fibers and Sensors for Medical Diagnostics and Treatment Applications XX (2020) 128–132.

[13] V. Budinski, D. Donlagic, Fiber-optic sensors for measurements of torsion, twist and rotation: a review, Sensors (Basel) 17 (3) (2017) 443–472.

[14] B. Audoly, Y. Pomeau, Elasticity and geometry: from hair curls to the non-linear response of shells, Oxford University Press, New York, 2010.

[15] R.C. Hibbeler, Mechanics of Materials, 8th ed., Pearson Prentice Hall, Upper Saddle River, New Jersey, 2011.

[16] R.J. Roesthuis, S. Janssen, S. Misra, On using an array of fiber Bragg grating sensors for closed-loop control of flexible minimally invasive surgical instruments, 2013 IEEE/RSJ International Conference on Intelligent Robots and Systems (2013) 2545–2551.

[17] J.V. Roosbroeck, C. Chojetzki, J. Vlekken, E. Voet, M. Voet, A new methodology for fiber optic strain gage measurements and its characterization, SENSOR+TEST Conferences, vol. OPTO 2 – Optical Fiber Sensors (2009) 59–64.

[18] F. Khan, A. Donder, S. Galvan, F. Rodriguez, S. Baena, Misra, Pose measurement of flexible medical instruments using fiber Bragg gratings in multi-core fiber, IEEE Sens. J. 20 (18) (2020) 10955–10962.

[19] J.J. Craig, Introduction to Robotics: Mechanics and Control, third ed., Pearson Prentice Hall, Upper Saddle River, New Jersey, 2005.

Biographies

Fouzia Khan studied Electrical Engineering and Control Systems at University of Toronto, Canada. Her doctoral research focused on utilizing fiber Bragg grating sensors for shape and pose sensing. The application of her research was for minimally invasive medical instruments. She was part of the Department of Biomedical Engineering at University of Groningen/University Medical Center Groningen, The Netherlands and a visiting researcher at University of Twente, The Netherlands.

David Barrera (Ph.D. 2013) is currently a Postdoc Researcher in the Department of Electronics at University of Alcalá. His current research interests include optical fiber sensors, fiber Bragg gratings, and multicore optical fibers.

Salvador Sales (Ph.D. 1995) is Professor at the in the ITEAM Research Institute, Universitat Politècnica de València, Spain, since 2007. He was recognized with the Annual Award of the Spanish Telecommunication Engineering Association to the best PhD. on optical communications. He has been involved some national and European research, and co-author of more than 250 journal paper His main research interests include optoelectronic signal processing, optical delay lines, fiber Bragg gratings, WDM and SCM lightwave systems and semiconductor optical amplifiers.

Sarthak Misra received the master's degree in mechanical engineering from McGill University, Montreal, QC, Canada, in 2001, and the doctoral degree in mechanical engineering from The Johns Hopkins University, Baltimore, MD, USA, in 2009. He is currently a Full Professor with the Department of Biomechanical Engineering, University of Twente, Enschede, The Netherlands, and also affiliated with the Department of Biomedical Engineering, University of Groningen, Groningen, Netherlands, and University Medical Center Groningen, Groningen, The Netherlands. Prior to commencing his doctoral studies, he was a Dynamics and Controls Analyst with the International Space Station Program. His research interests include surgical robotics and medical microrobotics. Prof. Misra was the recipient of the European Research Council Starting, Proof-of-Concept, and Consolidator Grants and the Netherlands Organization for Scientific Research VENI and VIDI Awards. He is a Co-Chair of the Robotics and Automation Society Technical Committee on Surgical Robotics and a Co- Chair of the International Federation of Automatic Control Technical Committee on Biological and Medical Systems.